Exploring the Differences between Forward Osmosis and Reverse Osmosis Fouling

Farrukh Arsalan Siddiqui [a,1], Qianhong She [b,c*], Anthony G. Fane [b,d], Robert W. Field [a**]

[a] Department of Engineering Science, University of Oxford, United Kingdom
[b] Singapore Membrane Technology Centre, Nanyang Environment & Water Research Institute, Nanyang Technological University, Singapore
[c] School of Chemical and Biomolecular Engineering, The University of Sydney, NSW 2006, Australia
[d] UNESCO Centre for Membrane Science and Technology, University of New South Wales, NSW 2052, Australia

[*] Corresponding author address: The University of Sydney, Room 494, Level 4, Chemical Engineering Building J01, Darlington, NSW 2006, Australia; Tel: +61 2 8627 6071; Fax: +61 2 9351 2854; Email: qianhong.she@sydney.edu.au

[**] Corresponding author address: University of Oxford, Parks Road, Oxford, OX1 3PJ, UK; Tel: +44 1865 273181; Fax: +44 1865 273010; Email: robert.field@eng.ox.ac.uk

[1] Permanent address: Department of Mechanical Engineering, Bahauddin Zakariya University, Bosan Road, Multan 60800, Pakistan

Abstract

A comparison of alginate fouling in forward osmosis (FO) with that in reverse osmosis (RO) was made. A key experimental finding, corroborated by membrane autopsies, was that FO is essentially more prone to fouling than RO, which is opposite to a common claim in the literature where deductions on fouling are often based solely on the water flux profiles. Our theoretical analysis shows that, due to a decrease in the intensity of internal concentration polarization (ICP), and thus an increase in the effective osmotic driving force during FO fouling tests, the similarity of experimental water flux profiles for FO and RO is in accordance with there being greater fouling in FO than RO. The specific foulant resistance for FO was also found to be greater than that for RO. Possible explanations are discussed and these include the influence of reverse solute diffusion from draw solution. Whilst this explanation regarding specific foulant resistance is dependent on the draw solution properties, the finding of greater overall foulant accumulation in FO is considered to be a general finding. Additionally, the present study did not find evidence that hydraulic pressure in RO plays a critical role in foulant layer compaction. Overall this study demonstrated that although FO has higher fouling propensity, it offers superior water flux stability against fouling. For certain practical applications this resilience may be important.

Keywords: forward osmosis; reverse osmosis; fouling; internal concentration polarization (ICP); cake-enhanced concentration polarization (CECP)

Graphic Abstract

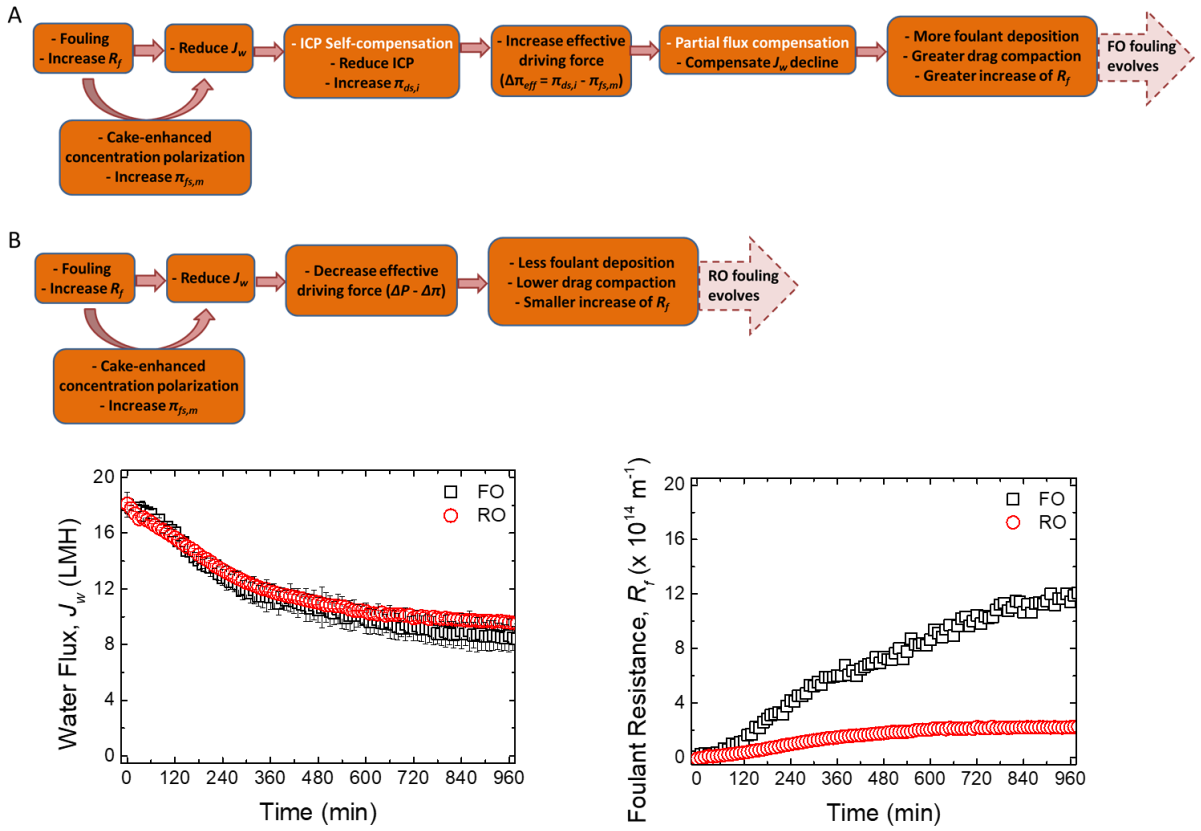

1. Introduction

Forward osmosis (FO) has received considerable interest in the recent decade for various applications such as desalination [1-4], wastewater treatment [3-6], trace contaminant removal [7-9], and resource recovery [10, 11]. In an FO process a draw solution (DS) with a higher osmotic pressure on one side of a selective membrane draws the water from a feed solution (FS) with a lower osmotic pressure on the other side of the membrane [1]. Unlike pressure-driven reverse osmosis (RO) that is a relatively energy-intensive process, osmotically driven FO process only requires minimum electrical energy for pumping the DS and FS solutions. In those special cases where the application does not require the regeneration of the DS (e.g., the osmotic dilution of the fertilizer-based DS [12] and/or the concentration of the FS for nutrient recovery [10]), FO has an outstanding advantage in terms of lower energy consumption. Also it has been suggested that a hybrid FO system that incorporates a DS regeneration process may also outperform conventional RO when treating challenging feedwaters (e.g., the feedwater with high salinity or specific challenging contaminants) [4, 13, 14]. Whilst energy consumption is a major factor in the evaluation between FO and RO [13, 15, 16], membrane fouling is another important consideration when comparing the performance of FO and RO in practical applications [3-5, 13, 14, 17].

1.1. Critical review of prior studies on the comparison of fouling in FO and RO

Owing to the different driving forces for FO and RO (i.e., osmotic pressure vs. hydraulic pressure), fouling behaviour between FO and RO has been presumed to be different. The comparison of membrane fouling between FO and RO processes has been studied extensively and it has been broadly claimed that osmotically driven FO has lower fouling tendency and greater fouling reversibility than pressure-driven RO [13, 18-28]. These studies attributed their claim to the lack of hydraulic compaction of the foulant layer in the FO process, which resulted

in the formation of different foulant layer structure in FO compared to that in RO. They stated that in FO the foulant layer is looser and less compacted and thereby the fouled membrane can be easily cleaned by a brief water rinsing, whereas in RO the foulant layer is densely compacted and tightly held on the membrane under the action of hydraulic pressure, thereby resulting in a reduced cleaning efficiency [19, 24].

On the other hand, a number of other studies have reported opposing observations [29-32]. Lay et al. did not observe differences in the flux decline between FO and RO fouling and they attributed this to the low initial water flux that was said to be below the critical flux [29], which today might be better termed threshold flux [33]. For alginate and silica fouling, Jang et al. observed in a laboratory study that fouling propensity was the highest for FO compared with RO and membrane distillation [30]. Tow et al. developed a method of *in situ* membrane fouling quantification and found greater foulant accumulation with FO than with RO, which suggests that fouling in FO might be more severe than RO despite the observed lower flux decline in FO [31]. In addition, their study did not find any evidence that the thinner cake layer (less foulant accumulation) in RO could be attributed to the hydraulic pressure compaction [31]. In an earlier study on alginate and silica fouling in RO under constant flux operation, Fane and Chong observed no clear difference in the trans-membrane pressure (TMP) profiles for a flux of 40 l/m^2hr (well above the critical flux for both foulants) with varying feed pressures from 22 to 30 bar, suggesting that foulant layer compaction is physically related to water flux not hydraulic pressure *per se* [32].

1.2. Analysis of possible reasons for the different findings on FO and RO fouling

The inconsistent findings on FO and RO fouling between different groups of researchers probably lie in the discrepancies with respect to experimental methods used, as well as in the

different analytical approaches. Firstly, in most of the prior studies experimental conditions for FO and RO were not comparably controlled. For example, (i) in many cases the apparent driving force for RO (i.e., hydraulic pressure, ΔP) was maintained constant during the entire RO experimental test, whereas that for FO (i.e., osmotic pressure difference between the bulk DS and the bulk FS, $\Delta\pi$) was gradually decreasing during the FO experimental test as the DS was gradually diluted and the FS was gradually concentrated [19-21, 23, 24, 30, 31, 34]; (ii) different types of membranes were used for FO and RO tests, for which different membrane properties may influence the fouling behaviour [26, 31]. Secondly, in many prior studies the reported water flux for RO was directly observed from experiments, whereas for FO it was not the experimentally observed flux but a corrected one by using experimental fouling flux and baseline flux under non-fouling conditions [19-24]. Typically, the approach to correct the observed FO flux was to eliminate the effects of DS dilution and the FS concentration during the test. However, the approach of flux correction did not take into account the effects of concentration polarization (CP) especially internal concentration polarization (ICP) that is strongly dependent on the solution concentration and will significantly influence the observed flux via the change in effective driving force [35-37]. Thirdly, the majority of prior studies compared the fouling propensity between FO and RO based on the extent of flux decline [19-24, 26, 30, 34]. However, in both FO and RO, especially FO, temporal changes in flux do not properly reflect the evolution of foulant accumulation on the membrane, because the flux decline is related not only to the hydraulic resistance of the foulant layer accumulated on the membrane but also to the CP that will result in the decrease of effective driving force [20, 31, 36-39]. It is also noted that the foulant layer formed on the membrane might influence the degree of external CP through the process of "cake-enhanced concentration polarization" [38]. Although Tow et al. developed a method to quantify membrane fouling by employing two parameters – cake structural parameter (that is related to cake-enhanced concentration

polarization) and pore hydraulic diameter (that is related to hydraulic resistance of foulant layer), it appears that their study only focused on the analysis of the former under conditions where cake hydraulic resistance is negligible [31].

1.3. Definition of fouling and objectives of the current study

The controversy over FO and RO fouling in prior studies has provided an impetus for us to perform an insightful comparison of fouling between FO and RO processes. It is noted that the majority of prior studies comparing fouling between FO and RO were based solely on the water flux profiles [18-26]. It was generally assumed that a water decline was an appropriate metric for fouling behaviour in both cases [18-26]. However, this overlooks a key difference between fouling in FO compared with that in RO. This is because water flux decline is dependent not only on fouling but also on driving force (i.e., osmotic pressure for FO and hydraulic pressure for RO), as shown below:

$$J = \frac{F}{\mu R} \quad (1)$$

where J is water flux, F is driving force, μ is viscosity of the solution, and R is the overall hydraulic resistance of membrane and foulant layer.

Now in this study we specifically define that *fouling* is the accumulation of foulant on the membrane, and is quantified by the foulant layer resistance (R_f), which is consistent with previous studies quantifying fouling of desalination membranes [32, 40-42]. As CP is flux dependent, fouling will change the effective driving forces in FO and RO because of changes in CP. Due to ICP changing with water flux, the changes in effective driving force are particularly significant for FO [36, 37]. Therefore, for FO processes, an examination of the decline in flux in isolation does not properly reflect the extent of fouling (i.e., the evolution of foulant accumulation on the membrane).

Consequently the current study aims to compare the fouling between FO and RO focusing on the comparison of hydraulic resistances of the foulant layers with due allowance for the CP effects. A specific objective is to have a mechanistic understanding of the differences of fouling and its influences on water flux between FO and RO. To enable a fair comparison our experiments were designed to use the same membranes, have essentially the same initial water flux, and have well controlled conditions including constant overall driving force, throughout the complete experiments as detailed in section 2.2.

2. Materials and Methods

2.1. Chemicals and membranes

Unless otherwise stated, all the chemicals used in this study were of analytical grade. Ultrapure deionised (DI) water which was supplied by a Milli-Q Ultrapure water system (Millipore Singapore Pte Ltd) with a resistivity of 18.2 MΩ cm was used to prepare all the solutions. Sodium salt of alginic acid (alginate, Sigma-Aldrich St. Louis, MO) was used as model foulant to study membrane fouling. It gives gel-layer fouling rather than cake-layer fouling but the term cake-enhanced concentration polarization (CECP) has been retained in this paper. The feed solution in both FO and RO fouling experiments was composed of 45 mM NaCl, 5 mM $CaCl_2$ and 200 mg/L alginate. The draw solution for FO experiments was composed of 1.5 M NaCl. The initial volume of the feed solution and draw solution was 5 L.

A cellulose triacetate (CTA) membrane provided by Hydration Technology Innovations (HTI, Albany, OR) was used in both FO and RO experimental tests. The CTA membrane comprised a dense selective layer and a porous support layer embedded within a polyester woven mesh fabric. This membrane has been widely used as a model membrane to compare fouling in FO and RO [19-21, 31]. The reason for the use of the same membrane in both FO and RO tests is

to eliminate the influence of membrane materials on fouling and thus generate a fair comparison between fouling in FO and RO.

2.2. FO and RO membrane fouling experiments

The same experimental setup was used for FO and RO experimental tests with only slight modification between the two different test modes (Fig. S1 in Supporting Information S1). This setup has also been used in our previous osmotic membrane fouling experiments and benefits, *inter alia*, from being able to maintain a constant draw concentration [43]. The setup had a PLC control system that allowed automatic control of experimental operation and data acquisition. For FO tests, both FS and DS were recirculated with Hydra-Cell positive displacement diaphragm pumps (Fig. S1A). The FO membrane test cell (CF042, Sterlitech Corporation) was comprised of two symmetric Delrin half-cells (top cell and bottom cell) with identical dimension of flow channel (85 mm length × 39 mm width × 2.3 mm height). A net spacer was placed in the DS flow channel to enhance the mixing and mass transfer of DS [44]. The DS cross-flow velocity was 11.1 cm/s. The draw solution conductivity (and thus concentration) was maintained constant by dosing with a more concentrated NaCl solution. The feed solution conductivity was monitored with time to estimate the reverse solute flux following the same methods described previously [44]. For RO tests, only FS was recirculated, while the permeate water was collected directly in a permeate tank (Fig. S1B). There was dosing of the feed with DI water to ensure concentration was kept constant. The RO membrane test cell had the same FS flow channel as that for FO. The permeate channel was filled with sintered porous metal plate (with ~20 μm mean pore size) that could fully support the membrane against deformation in the RO test. The feed and permeate conductivity were monitored with time to estimate the rejection.

For both FO and RO tests, the FS tank was placed on a digital balance and the FS mass (and thus FS volume and foulant concentration) was maintained constant via continuous dosing with DI water (see Fig S1B). Small amounts of salt leakage did occur from the DS side but the increase in bulk FS concentration was marginal due to large volume (5 L) of FS used in the experiments and its influence on the bulk DS and FS osmotic pressure difference is negligible according to conductivity monitoring. The mass change of the DI water with time was recorded and used to determine the water flux. No feed spacer was placed in the FS channel to accelerate fouling. The membrane active layer was facing the FS. The cross-flow velocity of FS was 7.4 cm/s. The apparent driving forces for both RO and FO (i.e., the applied hydraulic pressure for RO and the osmotic pressure difference between the bulk DS and the bulk FS for FO) were maintained constant.

After each fouling test, the fouled membrane was either cleaned via surface flushing to investigate the fouling reversibility or autopsied to determine the foulant deposition. During surface flushing, the FS was replaced with DI water and the cross-flow velocity of FS was increased to 29.6 cm/s. For the FO fouled membrane the DS was also replaced with DI and not recirculated; for the RO fouled membrane the applied hydraulic pressure was reduced to zero. In both cases the surface flushing was performed for 30 minutes. The foulant mass load (i.e., amount of foulant deposited on unit area of membrane surface) was determined by foulant extraction followed by measurement of the total organic carbon (TOC) using a similar protocol reported elsewhere [43]. The protocol is briefly summarized in Supporting Information S2.

2.3. Determination of foulant resistance for fouled membranes in FO and RO

Before the determination of the foulant resistance on the fouled membranes (R_f), the clean membrane resistance (R_m) was first measured via a RO test using a foulant-free feed solution

with the same background electrolyte used for the fouling test. The R_m for the clean membrane was estimated using the following osmotic-resistance filtration (ORF) model for RO that was reported elsewhere [45] and can be simplified from the universal ORF model for osmotically driven membrane processes (ODMPs) ([37] and Appendix A).

$$J_w = \frac{\Delta P - \eta_{rej}\pi_{fs} exp\left(\frac{J_w}{k_{ecp}}\right)}{\mu R_m} \quad (2)$$

where ΔP is the effective applied hydraulic pressure, η_{rej} is the solute rejection that was determined based on conductivity measurement of permeate and feed water, π_{fs} is the osmotic pressure of the feed solution (that can be correlated by the van't Hoff equation $\pi = C\beta R_g T$ where C is concentration, β is van't Hoff coefficient, R_g is the universal gas constant and T is temperature), J_w is the water flux, k_{cecp} is the mass transfer coefficient near the membrane surface, and μ is the viscosity of the feed solution. The membrane resistance R_m is related to the water permeability coefficient (A) by $A = 1/\mu R_m$. Note that external concentration polarization (ECP) has been incorporated in Eq. (2) and that for the feed channel k_{ecp} can be estimated following the approach reported elsewhere [46].

The structural parameter (S) of the FO membrane was determined by inputting π_{ds} and π_{fs}, and the foulant-free experimentally obtained parameters (i.e., J_w, J_s/J_w, R_m) into the following equation that is rearranged from the ORF model [37].

$$S = \frac{D}{J_w} \ln\left[\frac{\pi_{ds} + \frac{J_s}{J_w}\beta R_g T}{\left(\pi_{fs} + \frac{J_s}{J_w}\beta R_g T\right) exp\left(\frac{J_w}{k_{ecp}}\right) + \mu R_m J_w}\right] \quad (3)$$

The value of k_{ecp} was the same value as that estimated for RO because the membrane cell for the FO tests and RO tests had the same feed-side flow channel hydrodynamics.

The foulant resistance (R_f) on the RO fouled membrane was determined by inputting π_{fs}, ΔP, and the experimentally obtained $J_{w,f}$, $\eta_{rej,f}$ into Eq. (4) which, through the term $k_{ecp,f}$, includes an adjustment for cake-enhanced concentration polarization (CECP).

$$J_{w,f} = \frac{\Delta P - \eta_{rej,f}\pi_{fs} exp\left(\frac{J_{w,f}}{k_{ecp,f}}\right)}{\mu\left(R_m + R_f\right)} \quad (4)$$

where $J_{w,f}$ is the fouling water flux, $\eta_{rej,f}$ is the membrane rejection during the RO fouling test, and $k_{ecp,f}$ is the overall mass transfer coefficient across the foulant layer and external concentration polarization boundary layer. As shown by Eq. (5) $k_{ecp,f}$ is dependent on both the external concentration polarization (ECP) and CECP at the feed side. Thus $k_{ecp,f}$ consists of two terms, one is related to the mass transfer within the foulant layer on the membrane (k_{ecp,f^*}) and the other to the ECP boundary layer above the foulant layer ($k_{ecp,0}$).

$$\frac{1}{k_{ecp,f}} = \frac{1}{k_{ecp,0}} + \frac{1}{k_{ecp,f^*}} = \frac{\delta}{D} + \frac{S_f}{D} = \frac{\overline{S_f}}{D} \quad (5)$$

where δ is the boundary layer thickness adjacent to the foulant layer and it can be estimated from k_{ecp} for an empty channel [46]; S_f is the structural parameter of the foulant layer that has an analogous definition to the membrane structural parameter [31]; $\overline{S_f}$ is the sum of δ and S_f and is defined as the overall effective thickness of the CP boundary layer that incorporates both CECP within the foulant cake layer and the external CP adjacent to the foulant layer. For the calculation of R_f, a range of $\overline{S_f}$ from 125 μm to 719 μm (where 125 μm is the ECP boundary layer thickness) was selected based on the nature of alginate fouling [47]. Clearly the CECP effect is negligible when $\overline{S_f} = 125\ \mu m$. The selected range of $\overline{S_f}$ was rationalized via the sensitivity analysis as detailed in Appendix B. The numerator of Eq. (4) represents the effective driving force for RO during fouling and is used to calculate the RO effective driving force.

The R_f on the fouled FO membrane was calculated using π_{ds}, π_{fs}, and the experimentally obtained parameters ($J_{w,f}$, $J_{s,f}/J_{w,f}$, R_m and S) based on the ORF model given below [37].

$$J_{w,f} = \frac{(\pi_{ds} - \pi_{fs}) - F_{ecp,f}\left(\pi_{fs} + \frac{J_{s,f}}{J_{w,f}}\beta R_g T\right) - F_{dcp}\left(\pi_{ds} + \frac{J_{s,f}}{J_{w,f}}\beta R_g T\right)}{\mu(R_m + R_f)} \quad (6)$$

where the external concentration polarization (ECP) factor, $F_{ecp,f}$, at the feed side and dilutive concentration polarization (DCP) factor, F_{dcp}, at the draw side are expressed by Eq. (7) and Eq. (8), respectively.

$$F_{ecp,f} = exp\left(\frac{J_{w,f}}{k_{ecp,f}}\right) - 1 \quad (7)$$

$$F_{dcp} = 1 - exp\left(-\frac{J_{w,f}}{k_{dcp}}\right) = 1 - exp\left(-\frac{J_{w,f}}{D/S}\right) \quad (8)$$

Eq. (6) incorporates the effect of reverse solute diffusion (i.e., J_s/J_w), internal concentration polarization (included in F_{dcp}), and cake-enhanced concentration polarization (included in $F_{ecp,f}$). The term $k_{ecp,f}$ in Eq. (7) was determined by Eq. (5) following similar approaches to those for RO. Although a precise value of $\overline{S_f}$ was not determined in this study, the selected range of $\overline{S_f}$ readily indicates the trend of the calculated R_f for FO and RO (also refer to Appendix B). The numerator of Eq. (6) represents the effective driving force for FO during the fouling test and is used to calculate the FO effective driving force. The effect of different scenarios of $k_{ecp,f}$ on the calculated R_f and effective driving forces for FO and RO fouled membranes will be evaluated and compared. ORF models show that the mass transfer limitation for RO (Eq. (4)) only lies on the feed side but for FO (Eq. (6)) it lies on both the feed and draw (permeate) sides which concurs with an earlier analysis [48]. As shown later ICP (or k_{dcp}) at the draw side plays a significant role in determining the difference between FO and RO fouling behaviours. It is important to note that the calculation of R_f for both FO and RO fouled membranes (Eq. (4) and Eq. (6)) is based on the experimentally measured parameters,

which is essentially similar to the method for calculating clean membrane resistance R_m (or clean membrane water permeability *A*) widely used in the research community [36, 41, 49, 50].

3. Results and Discussion

3.1. Comparison of water flux performance between FO and RO

For both FO and RO tests, the initial water flux was controlled at the same level of ~18 LMH and the respective overall driving forces were maintained constant. Prior to fouling tests, baseline tests without adding foulant in the FS were performed. The results show that baseline fluxes for both FO and RO were almost constant during the entire test (Fig. S2 in Supporting Information S3). Therefore, the flux decline during the fouling test is solely due to the addition of foulant in the FS.

Fig. 1 shows the water flux behavior during FO and RO fouling tests and flux recovery after membrane cleaning by water flushing. As shown in Fig. 1a, the water flux decline due to membrane fouling in both FO and RO followed nearly the same trend. Similar observations have been reported previously [19, 21, 24]. After the physical cleaning, water fluxes for both FO and RO recovered significantly (Fig. 1b) with water flux recovery values of ~94% for FO and ~96% for RO. Given the error bars the difference is not statistically significant. This observation is different from that reported in previous studies in which flux recovery in FO was generally much greater than that in RO [19-22, 24, 51]. Our results show that FO and RO can have similar water flux decline trends during fouling and similar water flux recovery after physical cleaning.

However, as introduced in Section 1, the water flux profiles alone do not reflect the extent of membrane fouling. The subsequent sections will provide an in-depth analysis of membrane fouling in both FO and RO via the comparison of R_f in both processes.

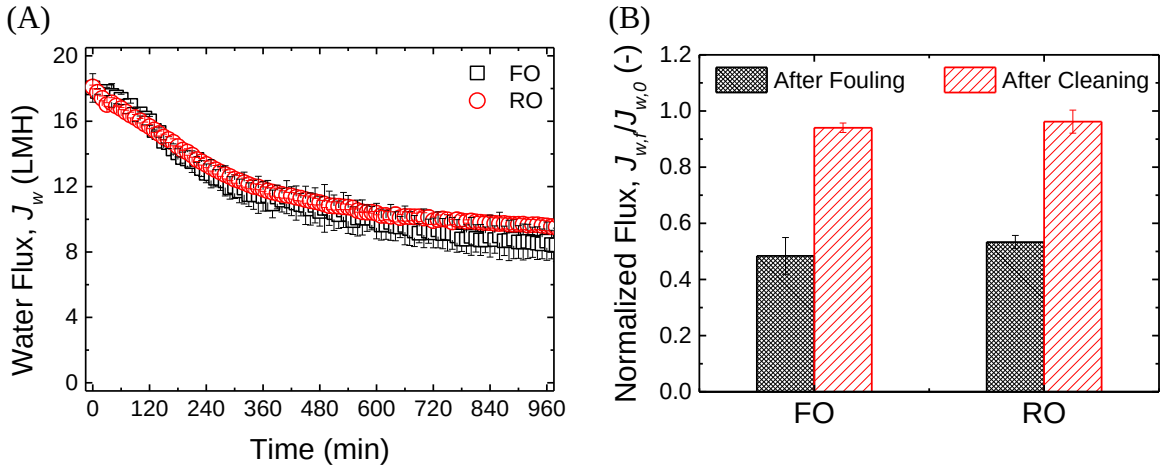

Fig.1. Comparison of FO and RO performance. (A) Water flux behavior during membrane fouling test, (B) water flux recovery after membrane cleaning. In the FO test DS was 1.5 M NaCl; in the RO test applied hydraulic pressure was 17.6 bar. Other fouling experimental conditions: FS contained 200 mg/L alginate, 45 mM NaCl and 5 mM $CaCl_2$; DS contained 1.5 M NaCl; no spacer was placed in FS flow channel, and a diamond net-type spacer was placed in DS flow channel; membrane active layer facing feed solution (AL-FS); cross-flow velocity in FS flow channel was 7.4 cm/s and that in DS flow channel was 11.1 cm/s. During membrane cleaning (surface flushing), the FS was replaced with DI water and cross-flow velocity increased to 29.6 cm/s for 30 minutes.

3.2. Comparison of fouling between FO and RO based on foulant resistance

Fig. 2 shows the foulant resistance R_f during FO and RO fouling calculated from the osmotic-resistance filtration models using the experimentally measured R_m of 3.26×10^{14} m^{-1}, S of 425 µm, $J_{w,f}$ from Fig. 1, specific reverse solute flux ($J_{s,f}/J_{w,f}$) for FO from Fig. S3 in Supporting Information S3, and rejection ($\eta_{rej,f}$) for RO from Fig. S4 in Supporting Information S3. The

calculation of foulant resistance R_f incorporated the effect of cake-enhanced concentration polarization as detailed in Appendix B. It was found that R_f for FO increased to a far greater extent than that for RO with the progress of fouling (Fig. 2a). At the end of the 16-hour fouling test, R_f for FO (~12.11×10^{14} m^{-1}) was over 5 times that for RO (~2.27×10^{14} m^{-1}). This comparison of foulant resistances reveals that for our experimental conditions FO is more prone to foulant accumulation than RO. More foulant accumulation in FO accords with the finding of Tow et al. who reported that S_f for FO would be increasingly greater than RO [31]. A sensitivity analysis of the effect of cake-enhanced concentration polarization on the calculated R_f was performed for different scenarios with $\overline{S_f}$ varying from 125 to 719 μm. It was found that the overall trend for all of the scenarios is similar to that in Fig. 2a (refer to Fig. B1 in Appendix B).

Fig. 2B shows that after physical cleaning the residual foulant resistance R_f for FO (~0.77×10^{14} m^{-1}) was also much greater than that for RO (~0.15×10^{14} m^{-1}), although water flux recovery for both processes was almost the same (Fig. 1B). This shows that basing conclusions solely upon a comparison of water fluxes, as is common e.g. [19-22, 24, 51], can be misleading. The trends of water flux (Fig. 1) and foulant resistance (Fig. 2) are reconciled in Section 3.4.

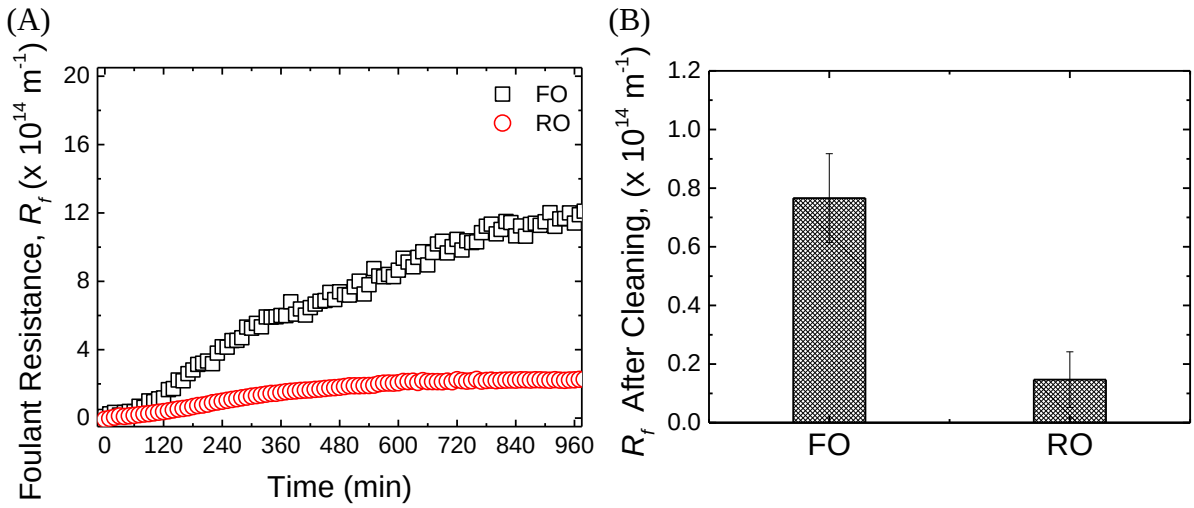

Fig. 2 – (A) Foulant resistance R_f during membrane fouling, and (B) Foulant resistance R_f after membrane cleaning. R_f was calculated based on the osmotic-resistance filtration models (Eq. (4) for RO and Eq. (6) for FO) using the experimentally measured water flux in Fig. 2, specific reverse solute flux (J_s/J_w) from Fig. S3 in Supporting Information S3 for FO, rejection for RO from Fig. S4 in Supporting Information S3, and basic membrane parameters (R_m and S), and incorporating the cake-enhanced concentration polarization.

To further examine the extent of fouling, the fouled membranes were autopsied to ascertain the foulant mass deposition density (m_f). As shown in Fig. 3a, at the end of the fouling test the amount of alginate depositing on the unit area of membrane surface for FO (~2.25 mg/cm^2) was nearly 2 times of that for RO (~1.24 mg/cm^2). Interestingly, the specific foulant resistance (R_f/m_f) as shown in Fig 3b indicates that the unit amount of alginate depositing on the membrane for FO caused greater hydraulic resistance than that for RO; R_f/m_f for FO (~5.40×10^{10} m/mg) is approximately 3 times of that for RO (~1.85×10^{10} m/mg).

(A) (B)

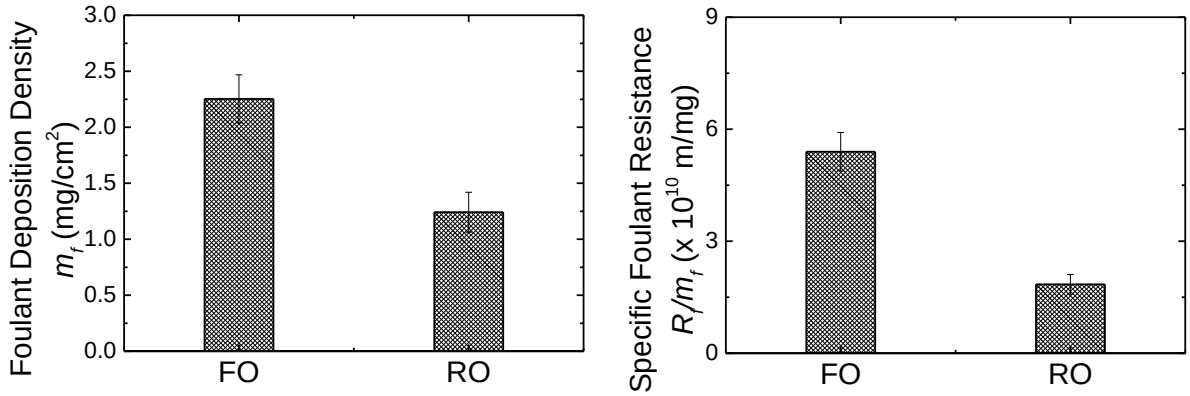

385 Fig. 3 – (A) Foulant deposition density, m_f; (B) Specific foulant resistance R_f/m_f. To calculate
386 the R_f/m_f , R_f was the value at the end of fouling test collected from Fig. 2.

387

388 That greater values of both m_f and R_f/m_f were observed for FO is contradictory to some previous
389 studies in which it is generally claimed that the foulant layer is less compacted in FO than RO
390 owing to the lack of hydraulic pressure in FO [19, 21-24]. Thus experiments specifically
391 designed to investigate the effect of hydraulic pressure on the compaction of the foulant layer
392 were undertaken, which is discussed later in Section 3.3.

393

394 With regard to the finding of greater values of both m_f and R_f/m_f for FO (in comparison to RO)
395 it is noted that this does accord with the findings of Song and Elimelech [52] who modelled
396 particle transport rates toward a nonporous membrane. They found a significant increase in
397 particle deposition upon an increase in salt concentration. Now in FO there is a significantly
398 higher salt concentration adjacent to the membrane due to reverse salt diffusion and so greater
399 particle deposition can be anticipated. Using experimental evidence provided by the work of
400 Sim et al. [53] it was shown that an increase in ionic strength of the feed solution leads to
401 increases in cake thickness and decreases in cake porosity which accords exactly with the
402 experimental findings reported above for FO. The mechanisms for fouling differences in FO
403 and RO are discussed in more detail in section 3.4.

404

3.3. Effect of hydraulic pressure on the compaction of foulant layer

As shown in Fig. S5 in Supporting Information S4, the experiment was divided into three stages: (1) foulant layer development stage, (2) solely hydraulic pressure compaction stage, and (3) performance re-evaluation stage. The test results are shown in Fig. 4. The first stage is the initial 4-hour constant-pressure (~17.6 bar) RO fouling test, at the end of which a foulant layer had formed on the membrane; the water flux had declined over 30%. In the second stage, the permeate valve was closed to ensure the permeate water flux was zero, thus eliminating the flux-induced hydrodynamic drag compaction and only leaving the hydraulic pressure (maintained at ~17.6 bar or elevated to ~27.6 bar) to "compact" the foulant layer for another 4 hours. In the third stage, the permeate valve was opened again and the permeate water flux was re-measured under the same pressure used in the first stage (~17.6 bar).

If the hydraulic pressure plays a more critical role in the "compaction" of the foulant layer than the water permeation drag force as previously claimed [24], then one would have expected to find upon reopening of the permeate valve that the hydraulic resistance of the foulant layer (R_f) had increased and the water flux had decreased. However, the opposite was found. As shown in Fig. 4 the water flux was elevated significantly after the fouled membranes had been solely "compacted" by the hydraulic pressure in the second stage. Importantly it was found that the level of the water flux elevation was independent of the pressure used to solely "compact" the foulant layer. The elevated water flux is likely to be due to the removal of some of the foulant layer by the cross-flow shear force in the absence of flux-induced drag. Our results suggest that it is the hydrodynamic drag force due to flux rather than the hydraulic pressure *per se* that plays a critical role in the compaction of the alginate fouling layer.

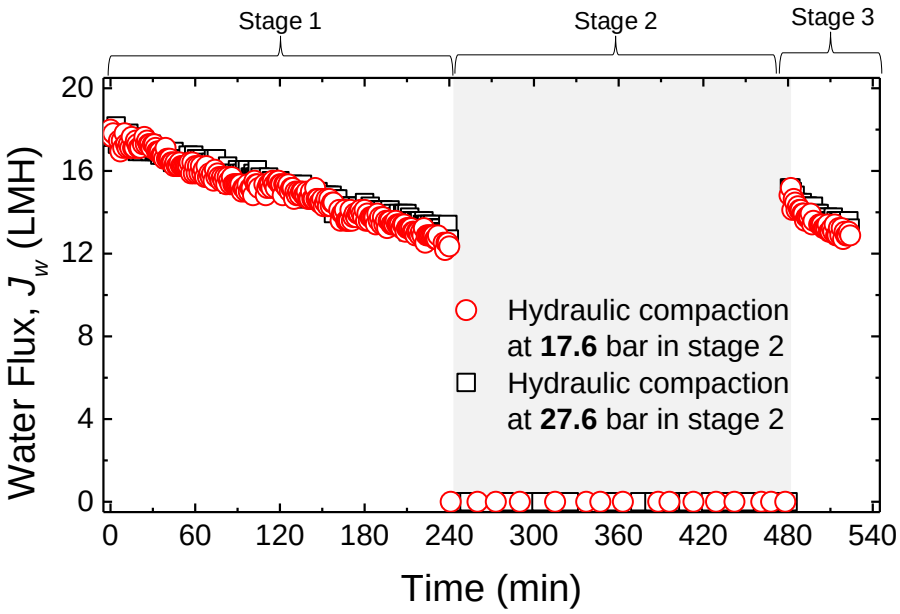

429

430 Fig. 4 – Effect of hydraulic pressure on the compaction of foulant layer. Water flux at different
431 stages is shown. Stage 1 is normal RO operation at 17.6 bar; in stage 2 foulant layer is
432 compacted only by hydraulic pressure at either 17.6 bar or 27.6 bar in which the permeate valve
433 is closed and permeate water flux is zero; in stage 3 the permeate valve is reopened and the
434 water flux is re-evaluated at 17.6 bar after the sole hydraulic compaction in stage 2. Other
435 experimental conditions: FS contained 200 mg/L alginate, 45 mM NaCl and 5 mM $CaCl_2$; no
436 spacer is placed in FS flow channel; cross-flow velocity in FS flow channel is 7.4 cm/s.

437

438 The above findings are in agreement with other previous studies [32, 54, 55]. When studying
439 RO and NF membrane fouling by humic acid [54], Tang and Leckie observed a limiting flux
440 that is independent of applied pressures (initial water fluxes) and membrane properties,
441 suggesting that the foulant layer compaction might not be dominated by pressure but by flux;
442 otherwise a limiting flux would not be observed. During the investigation of RO membrane
443 fouling under constant-flux operation (see Fig. S6 in Supporting Information S4) and [32],
444 Fane et al. found no clear difference in TMP profiles with varying feed pressure for either silica
445 or alginate fouling as long as the water flux was maintained constant. They concluded that cake

filtration is related to the differential pressure across the fouling layer that is physically related to flux (Eq. (4)) rather than to the absolute pressure itself [56]. In a recent study Tow and Lienhard found that alginate gel compaction by high feed hydraulic pressure does not occur and suggested that other explanations should be sought for FO's fouling resistance relative to RO [55]. In the following sections we will explore further the mechanisms governing the different fouling behaviours between FO and RO observed in this study.

3.4. Mechanisms for the different fouling behaviours between FO and RO

3.4.1. ICP self-compensation effect

The difference in foulant accumulation between FO and RO can be attributed primarily to the different responses of their driving forces to the water flux. For FO the effective osmotic driving force is significantly influenced by the ICP that is exponentially proportional to the water flux [35, 36]. A small variation of water flux can result in a significant variation of ICP and thus effective driving force [36]. Fig. 5 shows the effective driving forces for FO and RO during the fouling tests. Despite the same effective driving force at the beginning of fouling tests, the effective driving force for FO increased significantly with the progress of fouling test, while that for RO slightly decreased. At the end of fouling test the effective driving force for FO became nearly three times of that for RO. In an earlier study of modelling the effective driving force for FO and RO under the same extent of fouling, Lay et al. also found that the effective driving force for FO was greater than that for RO [29].

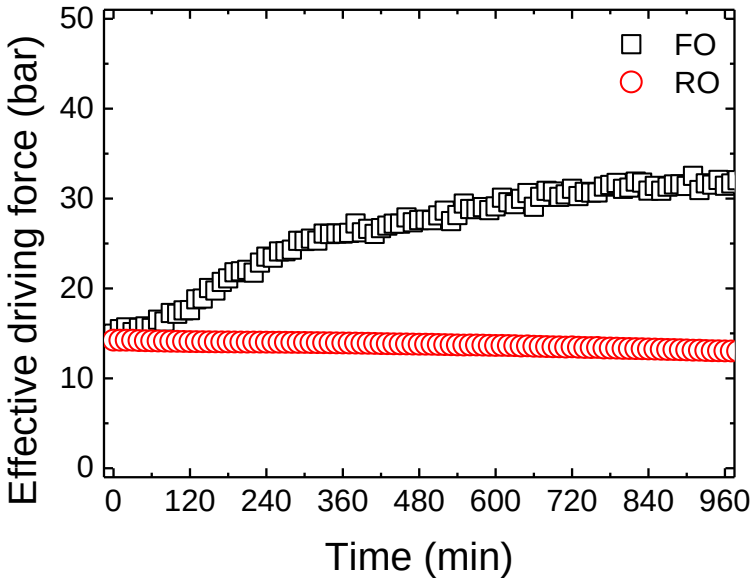

Fig. 5 – Comparison of effective driving force in FO and RO during the fouling test. Effective driving force is the numerator of osmotic-resistance filtration models (Eq. (4) for RO and Eq. (6) for FO) and is calculated using the experimentally obtained water flux in Fig. 2, specific reverse solute flux (J_s/J_w) from Fig. S3 in Supporting Information S3 for FO, rejection for RO from Fig. S4 in Supporting Information S3, and basic membrane parameters (R_m and S), and incorporating the cake-enhanced concentration polarization.

The progressively increased effective driving force in FO is due to the ICP self-compensation effect [36, 37]. That is, the decreased water flux due to membrane fouling results in a decrease in ICP, which in turn leads to an increase in the effective osmotic driving force. The different evolution of fouling in FO and RO is elaborated through simulation as discussed in detail in Section 3.5 and as shown in Fig. 8 later. Here a pictorial explanation is given. Although there are not discreet steps, one can view the evolution of the flux decline as consisting of a number of components as depicted in Fig. 6A. The increase in the effective driving force in FO leads to partial flux compensation which in turn leads to greater foulant accumulation. More accumulation leads to a further decrease in water flux and with the decreased water flux (and

484 the consequent ICP self-compensation) the process continues until there is a balance between
485 foulant being convected to the surface and foulant being removed by crossflow.
486
487 In contrast, the effective driving force for RO (i.e., the difference between the hydraulic
488 pressure and the osmotic pressure) responds much less significantly to the change of water flux,
489 noting that in RO only external CP changes with flux but hydraulic pressure is maintained
490 constant. It could even decrease with the progression of fouling due to increased cake-enhanced
491 concentration polarization (Fig. 6B). Thus, the compensation for partial flux decline is much
492 weaker or does not exist for RO. Consequently, the increase of foulant resistance for RO is
493 much smaller than that for FO (Fig. 2A) and the foulant deposit in RO is smaller than FO (Fig.
494 3A).
495
496 The evolution of foulant accumulation (R_f) can also be explained mathematically by
497 differentiating the water flux equation $J = F/\mu R$ with respect to time (t), which is easy to show
498 that
499 $$\frac{dR/dt}{R} = \frac{(-dJ/dt)}{J} + \frac{dF/dt}{F} \quad (9)$$
500 where J is water flux, F is driving force, and R is resistance. Thus the relative increase in
501 resistance at any point during the evolution of the resistance is the sum of the relative flux
502 decline and the relative increase in driving force. In the case of RO the third term is negligible
503 or very small but in the case of FO it is not. Therefore for the similar water flux decline profile,
504 the increase in resistance for FO is increasingly greater than RO.
505
506 It is well known that for a compressible filter cake that the porosity at the bottom, i.e., nearest
507 the support (it is membrane in our case), is lowest. This is because the bottom layers of the
508 cake have to support the drag forces imparted on the top layer of the cake. If there is more drag

(due to larger deposit and R_f as in FO at compensated partial flux), the bottom of the cake is more compressed. Our measured specific cake resistance is the cake average value, but this may be dominated by the effect of the bottom layer. This offers a partial explanation for the greater specific cake resistance for FO than RO (Fig. 3B) or more exactly an explanation for augmentation of the higher specific cake resistance. This might also explain that, under the same surface flushing conditions, the residual foulant resistance for FO fouled membrane was greater than RO fouled membrane (Fig. 2B), since the bottom cake layer might dominate the overall specific cake resistance. A second reason for higher specific resistance in FO is that the diffusiophoretic gradient is higher within the cake layer [57] due to reverse solute diffusion and as noted in this previous study this could lead to cake compaction by diffusiophoresis (DP); this will be discussed further in Section 3.4.3.

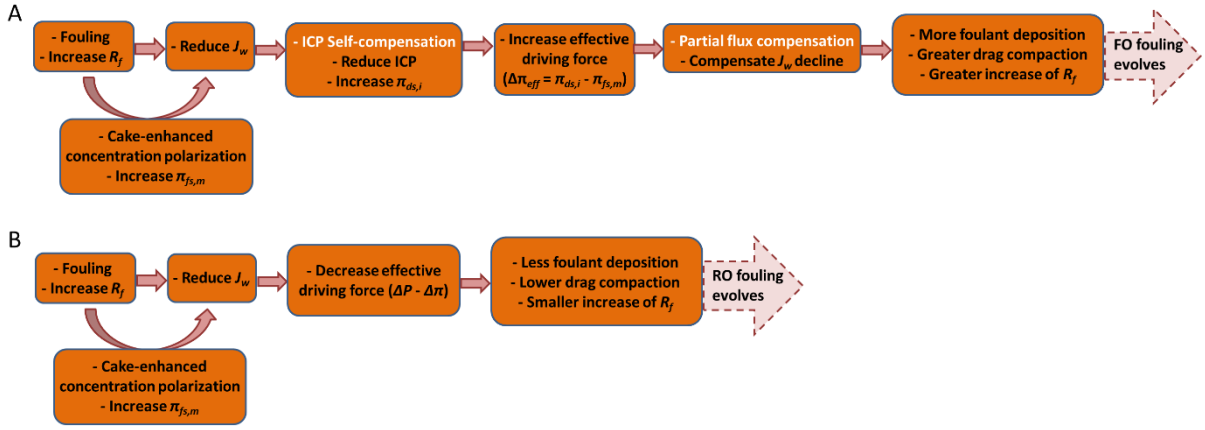

Fig. 6 – Evolution of membrane fouling in (A) FO and (B) RO. The relationship linking fouling, water flux, ICP self-compensation, cake-enhanced concentration polarization (CECP), and effective driving forces in FO and RO is schematically illustrated.

3.4.2. Cake-enhanced concentration polarization (CECP)

The results in Fig. 5 on the analysis of effective driving force also suggest that cake-enhanced concentration polarization (CECP) might play a less important role in FO in the AL-FS orientation compared to that in RO for the alginate fouling in this study. For RO, CECP could

result in the decrease of effective driving force that further aggravates the decrease of water flux. However, for FO, CECP would not change the trend where the effective driving force tends to increase with the progress of fouling. The reasoning again relates to the ICP self-compensation effect – the decreased ICP at the draw side due to the decrease of water flux by fouling was much more significant than the cake-enhanced CP at the feed side in this study. This was further demonstrated through sensitivity analysis for a wide range of scenarios - see Fig. B1b in Appendix B. This shows that the increase of effective driving force for FO could be moderately slowed down at an increased CECP, but the overall trend (effective driving force for FO significantly > RO) remains unchanged as long as the fouling continues to lead to an increase of foulant resistance (R_f). This finding supports an earlier study on the modelling of the effect of feed concentration on FO water flux, where She et al. suggested that CECP might not be important for FO in the AL-FS membrane orientation due to the strong ICP self-compensation effect [37].

3.4.3. Reverse solute diffusion (RSD)

The reverse diffusion of draw solute into the FS can influence the fouling behaviour (either increasing or decreasing fouling) due to the change of local feed solution chemistry near the FO membrane surface, which has been identified to be a unique fouling mechanism for osmotically driven membrane processes [37, 43, 44]. In the current study the reverse diffusion of NaCl from DS into FS would elevate the ionic strength of FS. As shown in Fig. 7, it was estimated, based on the approach reported previously [58, 59], that the local ionic strength near the active layer surface was elevated from ~98 mM at the beginning to ~167 mM at the end of the fouling test due to both CECP and reverse solute diffusion (RSD). In comparison, during the RO fouling test the bulk FS ionic strength is constant (~60 mM) and the local ionic strength near the active layer surface was elevated from ~86 mM to ~117 mM due to CECP. It has been

554 reported that with an increased ionic strength, the alginate fouling rate reduces when the feed
555 solution has a high Ca^{2+} concentration (> 1 mM) [60, 61] due to the reduced binding affinity
556 between Ca^{2+} and carboxyl units of the organic compounds [60-63]. Owing to the relatively
557 high Ca^{2+} concentration (5 mM) in the feed solution in the present study, it was expected that
558 the increased ionic strength at the feed side in FO due to reverse diffusion of NaCl could lead
559 to a decreased specific cake resistance. However experimental results in Fig. 2 show that the
560 specific cake resistance as well as the overall foulant resistance was greater for FO compared
561 with RO. This suggests there would be other reasons. In addition to the ICP self-compensation
562 as discussed in Section 3.4.1, another potential contributing effect is diffusiophoresis (DP) [57].
563
564 In FO, due to RSD, there would be a steeper concentration gradient of salinity across the foulant
565 layer, which aligns with estimates in Fig 7. This would invoke a stronger diffusiophoresis (DP)
566 effect in FO than RO, particularly if the feed solution is of low salinity. This stronger effect in
567 FO may not only lead to a great specific resistance but could also augment the degree of
568 deposition. Whilst the greater foulant load in FO compared to RO is definitely due in part to
569 the decrease in the intensity of ICP with time, and hence the increase in effective driving force,
570 it may be augmented by DP. Previous work has shown that the critical flux for a feed consisting
571 principally of humic acid had a lower value with an RO membrane compared to the value for
572 a UF membrane. (Taheri paper JMS 2015). Now this was partially attributed to DP because
573 for the RO membrane (unlike the UF one) salt gradients would be established. The plateau
574 fluxes in Fig. 1 (which can be taken as a measure of the critical fluxes) are lower for FO than
575 RO by around 10-15% and this accords with DP having a potential role in determining the net
576 flux of foulants towards the membrane surface.
577

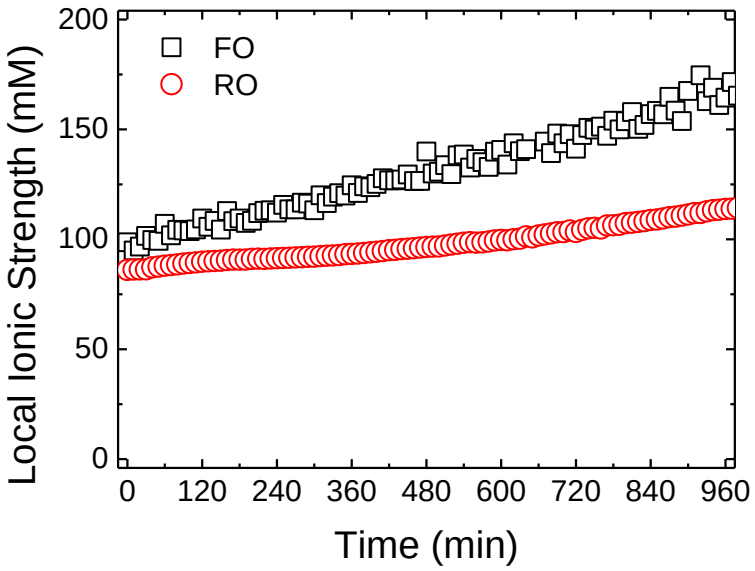

578

579 Fig. 7 – Estimated local ionic strength near the membrane active layer surface for FO and RO
580 during the fouling test. The calculation of local ionic strength followed the method reported
581 previously [58, 59] incorporating cake-enhanced concentration polarization.

582

583 **3.5. Implications**

584 The above experimental results show that although FO is more prone to fouling in terms of
585 more foulant accumulation and greater foulant hydraulic resistance than RO, the water flux in
586 FO might be more stable against fouling, which could enable FO to be a more resilient process
587 in some applications. This is further elaborated in this section by the simulation of FO and RO
588 water fluxes as a function of the extent of fouling (i.e., foulant resistance) in Fig. 8. The slope
589 of Fig. 8 was mathematically derived in Appendix C to further help the analysis of the fouling
590 behaviour. For the same extent of fouling (i.e., at the same R_f when $R_f > 0$) it is apparent that
591 the water flux for FO is intrinsically higher than that for RO, demonstrating the superiority of
592 FO to RO in terms of water flux performance. However, the same extent of fouling will not be
593 a stable condition in a practical operation. This is because a higher flux in FO under such
594 conditions would bring more foulants towards the membrane and lead to a greater
595 hydrodynamic drag force, which would result in more foulant accumulation in FO and in turn

more flux decline, as exhibited in our experimental observations (see Sections 3.1 and 3.2). Fig. 8 also shows that at the same level of water flux during fouling tests the foulant resistance for FO has to be greater than that for RO. This concurs with our experimental observations in Section 3.2. As illustrated in Fig. 8, in some cases FO can exhibit higher flux even at more severe fouling (e.g., water flux of FO at foulant resistance of $R_{f,2}$ is greater than that of RO at $R_{f,1}$).

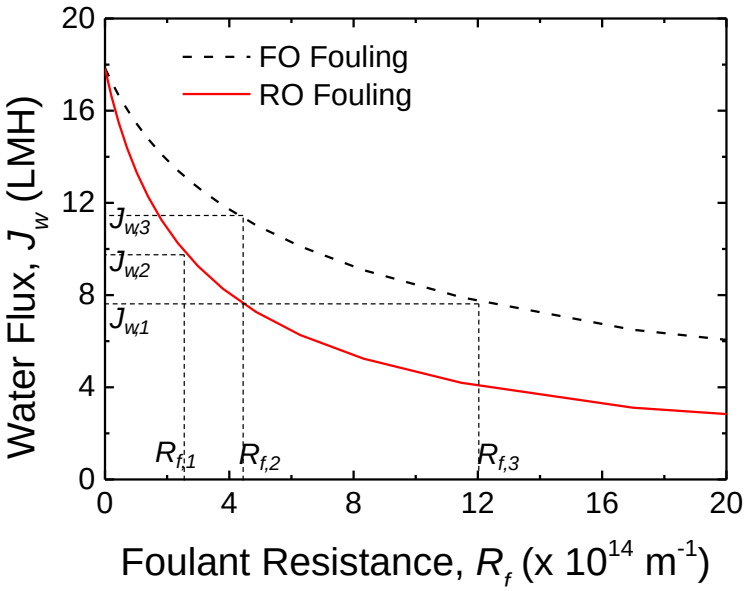

Fig. 8. Simulation of water flux of FO and RO as a function of foulant resistance. The simulation is based on the osmotic-resistance filtration models (Eq. (4) and Eq. (6)) assuming that membrane fouling only leads to the increase of R_f while other membrane parameters (solute permeability coefficient B value and structural parameter S value) are unchanged. Cake-enhanced concentration polarization (CECP) is considered in the simulation by assuming $\overline{S_f}$ increases from 125 μm to 500 μm. For the clean membrane the R_m is 3.26 × 10^{14} m^{-1}, the B value is 4.47 × 10^{-7} m/s, and the S value is 425 μm.

During membrane cleaning, the water flux for FO can be recovered to a higher level than RO even though the fouled FO membrane is not cleaned to the same extent as the fouled RO membrane. This point is illustrated in Fig. 8. Considering that the foulant resistance for FO is

614 reduced from $R_{f,3}$ to $R_{f,2}$ after membrane cleaning (Fig. 8), the water flux for FO will still be
615 greater than that for RO when the foulant resistance is reduced from $R_{f,2}$ to $R_{f,1}$ in Fig. 8. Again
616 this indicates that the change of water flux in FO in response to a given change of foulant
617 resistance (i.e. fouling) is much less than that in RO. This also explains why fouling
618 reversibility, based on measured water fluxes, appears to be more effective for FO than RO
619 [19-25, 27]. This is not due to the foulant layer in FO being less compacted (indeed on the
620 contrary we found the specific resistance to be higher for FO) but because the change in ICP
621 (and thus the change in effective driving force) in FO leads to a higher flux in the presence of
622 residual fouling.
623
624 The above modelling does not incorporate the influence of diffusiophoretic deposition (DP).
625 As elegantly illustrated in Fig.9 of their paper, Guha et al [57] showed that for filtration-based
626 particle deposition leading to convective cake formation one can often expect filtration-based
627 ion concentration polarization which leads to diffusiophoretic movement augmenting particle
628 deposition and this in turn creates both a greater level of cake formation and compaction, and
629 further enhanced ion concentration polarization. Thus there is a positive feed-back loop further
630 enhancing fouling.
631
632 In summary, the advantage of greater water flux stability of FO over RO is due to the ICP self-
633 compensation effect for FO that can result in a partial water flux compensation and leverage
634 the water flux decline by increasing the effective driving force. Our results suggest that,
635 contrary to earlier reports, FO does not benefit from less foulant compression due to its low
636 hydraulic pressure operation. While ICP is generally regarded as a detrimental effect for FO,
637 the current study reveals that ICP can also have an upside in that it helps to maintain water flux
638 stability. An interesting corollary to this is that the quest for FO membranes with smaller and

639 smaller *S* values to reduce ICP needs to consider whether there is an optimal *S* value that
640 balances the magnitude of flux decline and the resilience that the ICP compensation imparts
641 upon the system.
642
643 **4. Conclusions**
644 In this study the differences in membrane fouling between FO and RO were explored under
645 comparably controlled experimental conditions in which the apparent driving forces for FO
646 and RO were maintained constant. Sodium alginate was the foulant. It was found that:
647 1. Water flux decline during both FO and RO fouling tests followed broadly the same trend
648 and water flux recovery after membrane cleaning for both FO and RO reached a similar
649 level. However, the driving forces of FO and RO respond differently to the progression of
650 fouling and as a result the foulant resistance for FO was increasingly greater than that for
651 RO.
652 2. Membrane autopsy after the fouling tests showed that more foulant had been deposited on
653 the FO fouled membrane than the RO fouled membrane. Also, the specific foulant
654 resistance was greater with FO than RO.
655 3. The dominant reason for the higher fouling propensity in FO is due to the change of ICP
656 and effective driving force in response to the evolution of fouling; it is true for all systems
657 with manifest ICP.
658 4. Calculations suggest that CECP does not play an important role in flux decline in FO due
659 to the dominance of the ICP self-compensation effect.
660 5. The reverse diffusion of draw solute into feed solution could also influence fouling in FO
661 in two ways. Firstly directly as a result in the change of feed solution chemistry, an effect
662 that is strongly dependent on the draw solution properties. Secondly RSD will also
663 influence the salinity gradient across the FO foulant layer. This gradient will be greater in

FO than the corresponding one for RO and probably led to diffusiophoresis (DP). The role of DP in FO is worthy of further investigation.

6. No evidence was found that hydraulic pressure in RO plays a critical role in the compaction of alginate fouling layers. Furthermore the generally observed high flux reversibility of FO after membrane cleaning is probably due to the change of ICP (and thus effective driving force) in response to fouling rather than the lack of compaction due to hydraulic pressure.
7. Overall and not withstanding its higher fouling propensity, FO was found to exhibit higher flux stability against membrane fouling. Excluding those applications where the reverse salt flux generates additional fouling FO is potentially a more resilient process than RO.

Acknowledgements

This research was supported by a grant from the Singapore National Research Foundation under its Environmental and Water Technologies Strategic Research Programme and administered by the Environment and Water Industry Programme Office (EWI) of the PUB under the project number: 1102-IRIS-07-01. Q.S. is grateful to the support of FEIT ECR and Newly Appointed Staff Funding Scheme at The University of Sydney. Professor Rong Wang and Professor Chuyang Tang are thanked for their valuable comments. F.A.S. is grateful to SMTC at NTU, Singapore for hosting a year-long research visit.

Appendix A. Derivation of osmotic-resistance filtration model for RO

The osmotic-resistance filtration model of Eq. (A1) is originally derived for osmotically driven membrane processes and differentiates all the driving forces incorporating concentration polarization and reverse solute diffusion [37].

$$J_w = \frac{(\pi_{ds}-\pi_{fs})-F_{ecp}\left(\pi_{fs}+\frac{J_s}{J_w}\beta R_g T\right)-F_{dcp}\left(\pi_{ds}+\frac{J_s}{J_w}\beta R_g T\right)}{\mu R_m} \quad \text{(A1)}$$

where F_{ecp} and F_{dcp} are the concentrative external concentration polarization (ECP) factor at the feed side and dilutive concentration polarization (DCP) factor at the draw side respectively. They are expressed by Eq. (A2) and Eq. (A3).

$$F_{ecp} = exp\left(\frac{J_w}{k_{ecp}}\right) - 1 \quad \text{(A2)}$$

$$F_{dcp} = 1 - exp\left(-\frac{J_w}{k_{dcp}}\right) = 1 - exp\left(-\frac{J_w}{D/S}\right) \quad \text{(A3)}$$

Eq. (A1) is also applicable for RO and can be expressed as Eq. (A4) considering the direction of water flux and solute flux as well as the redefinition of signs to represent the parameters for RO.

$$J_w = \frac{\Delta P - (\pi_{fs} - \pi_p) - F_{ecp}\left(\pi_{fs} - \frac{J_s}{J_w}\beta R_g T\right)}{\mu R_m} \quad \text{(A4)}$$

At equilibrium DCP does not exist in RO and the specific solute flux ($\frac{J_s}{J_w}$) can be correlated to the permeate concentration (c_p) by Eq. (A5).

$$c_p = \frac{J_s}{J_w} \quad \text{(A5)}$$

Inserting Eq. (A2) and Eq. (A5) into Eq. (A4) yields the expected equation:

$$J_w = \frac{\Delta P - (\pi_{fs} - \pi_p) exp\left(\frac{J_w}{k_{ecp}}\right)}{\mu R_m} \quad \text{(A6)}$$

By assuming that the concentration and osmotic pressure follow the van't Hoff equation, the solute rejection in RO can be expressed below.

$$\eta_{rej,f} = 1 - \frac{C_p}{C_f} = 1 - \frac{\pi_p}{\pi_f} \quad \text{(A7)}$$

Inserting Eq. (A7) into Eq. (A6) yields

$$J_w = \frac{\Delta P - \eta_{rej}\pi_{fs} exp\left(\frac{J_w}{k_{ecp}}\right)}{\mu R_m} \quad \text{(A8)}$$

Appendix B. Sensitivity analysis of the effect of cake-enhanced concentration polarization (CECP) on the calculated values of foulant resistance R_f

This section shows the results of a sensitive analysis in which the influence of assumed levels of cake-enhanced concentration polarization (CECP) on the calculated R_f for FO and RO were explored. R_f was calculated for the following four scenarios using the experimentally measured data (i.e., J_w, J_s/J_w, R_f, S, π_{ds} and π_{fs}).

- Case (1): ECP at the feed side is neglected (i.e., assuming $\overline{S_f} = 0$ in Eq. (5)).
- Case (2): ECP at the feed side is considered but CECP is neglected (i.e., assuming $S_f = 0$ and $\overline{S_f} = \delta$ in Eq. (5); using $\overline{S_f}$ of 125 μm that is estimated for empty flow channel following the method reported elsewhere [46]).
- Case (3): CECP is considered and S_f is the same for both FO and RO (i.e., assuming that $\overline{S_f}$ for both FO and RO increases at the same rate with the progress of fouling test from 125 μm at the beginning of fouling test to 422 μm at the end of fouling test).
- Case (4): CECP is considered and S_f for FO becomes increasingly greater than that for RO based on the analysis of Tow et al. [31] (i.e., $\overline{S_f}$ for FO increases faster with the progress of fouling than that for RO; specifically it was assumed that $\overline{S_f}$ for FO increases from 125 μm to 719 μm whilst that for RO increases from 125 μm to 422 μm during the fouling tests).

As shown in Fig. B1a, for all the scenarios R_f for both FO and RO increased with the progress of fouling test. Moreover, although the increase of concentration polarization from Case (1) to (4) at a fixed time could decrease the calculated R_f for both FO and RO, for all scenarios R_f for FObecomes increasingly greater than that for RO. Note that for Case (4) the selected range of $\overline{S_f}$ for FO from 125 μm to 719 μm over the testing period approaches an extreme condition in which a further faster increase in $\overline{S_f}$ (i.e. a more severe rate of foulant accumulation) would

result in a decrease in the calculated R_f (see Fig. B1c for Case (5)) which is unrealistic. In addition, the assumption of a faster increase of $\overline{S_f}$ for FO in Case (4) has already suggested that foulant accumulation for FO is more severe than that for RO [31]. As there is much greater R_f for FO with the progress of fouling, these results further corroborate our observation that FO has a greater fouling propensity than RO even under the extreme conditions considered here. Although a more valid method needs to be developed to determine the accurate $\overline{S_f}$ value, the sensitive analysis with $\overline{S_f}$ varying within the boundary conditions can clearly demonstrate that R_f for FO is always greater than RO under the experimental conditions in the current study.

(a)

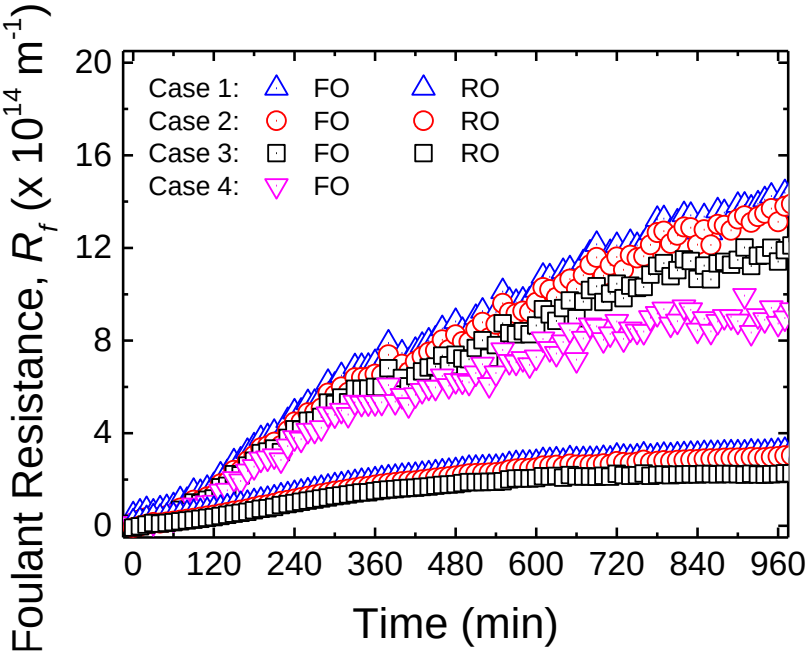

(b)

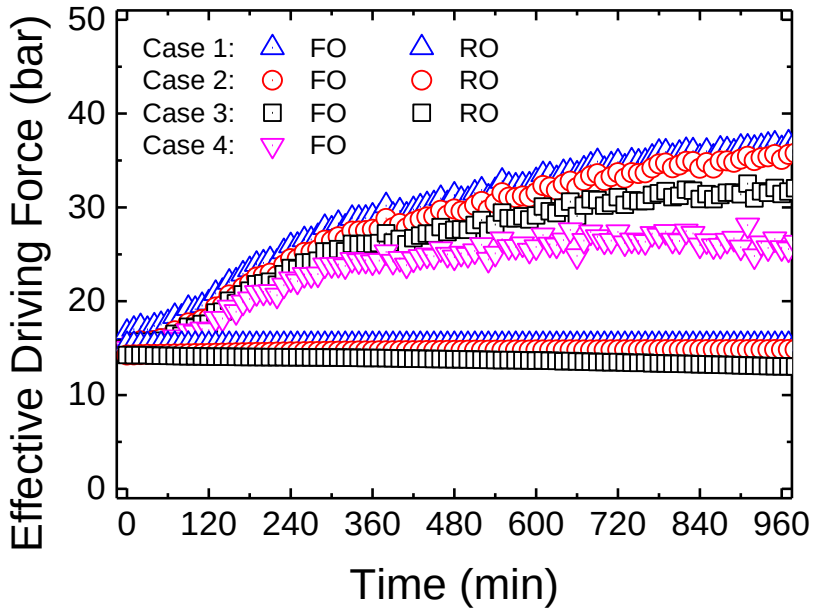

(c)

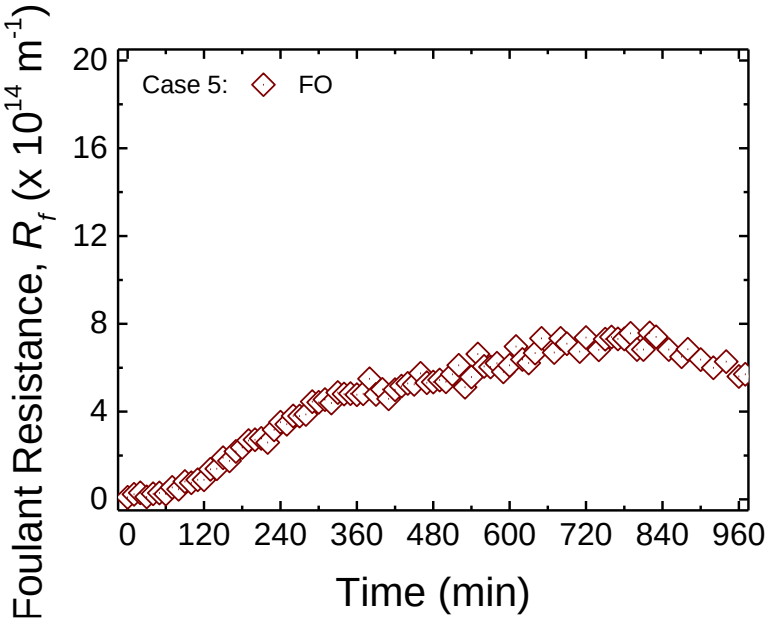

Fig. B1 – Calculated foulant resistance (R_f) (a) and effective driving force (b) for FO and RO based on the osmotic-resistance filtration model in different scenarios: (1) cake-enhanced concentration polarization (CECP) is neglected (i.e., assuming that the ECP boundary layer thickness (δ) is zero), (2) CECP is considered but cake-enhanced concentration polarization is neglected (i.e., using δ of 125 μm that is estimated for empty flow channel following the method reported elsewhere [46]), (3) CECP is considered and the foulant layer structural parameter (S_f) is the same for both FO and RO (i.e., $(\delta + S_f)$ for both FO and RO increases at the same rate with the progress of fouling test from 125 μm at the beginning to 422 μm at the end of fouling test), and (4) CECP is considered and the foulant layer structural parameter (S_f) for FO becomes increasingly more greater than that for RO (i.e., $(\delta + S_f)$ for FO increases faster with the progress of fouling than that for RO; $(\delta + S_f)$ for FO increases from 125 μm to 719 μm, while that for RO increases from 125 μm to 422 μm). For the calculation, the

764 experimentally obtained clean membrane resistance R_m is 3.26 × 10^{14} m^{-1} and structural
765 parameter S is 425 μm. (c) foulant resistance (R_f) for case (5) when the $\overline{S_f}$ has a faster increase
766 than that in case (4).
767

768 Fig. B1b shows the effective driving force for FO and RO. For all the Cases the effective
769 driving force for FO increased with the progress of fouling test and became increasingly greater
770 than that for RO. In contrast to FO, the effective driving force for RO behaved differently for
771 different scenarios: it maintained constant for Case (1), increased gradually with fouling test
772 for Case (2), and decreased gradually with fouling test for Case (3). Although the increase of
773 concentration polarization from Case (1) to Case (4) led to the decrease of effective driving
774 force for both FO and RO at a fixed time of fouling test, the effective driving force for FO was
775 always increasing with the fouling test and becoming increasingly greater than that for RO.
776 This suggests that (1) the different response of the effective driving force to fouling test
777 between FO and RO is the major reason for their different fouling behaviours, and (2) CECP
778 for FO plays a much less important role in flux decline than it does for RO.
779

780 Fig. B2 shows the calculated specific foulant resistance (R_f/m_f) using the experimentally
781 measured foulant deposition density (m_f) and calculated R_f in Case (4) that is under the
782 extreme conditions. Interestingly, the specific foulant resistance (R_f/m_f) for FO is still
783 consistently greater than RO even under the case of extreme conditions.
784

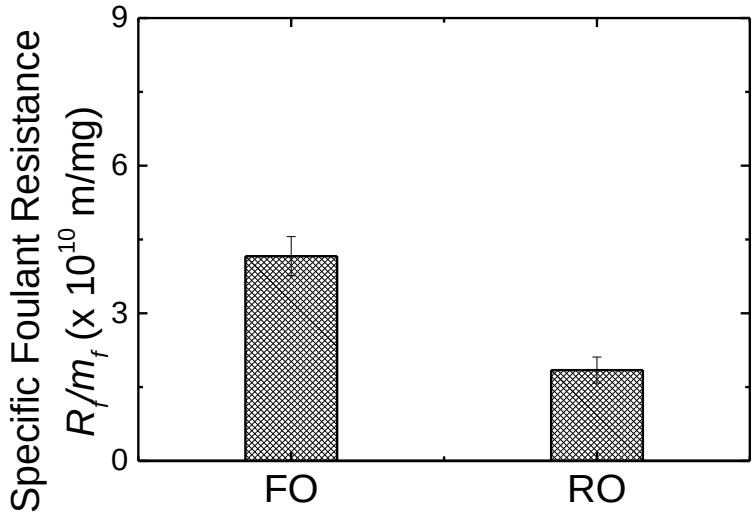

Fig. B2 – Specific foulant resistant (R_f/m_f) for FO and RO. R_f/m_f was calculated using the R_f from Fig. B1a in Scenario (4) and the experimentally measured m_f in Fig. 3A.

Appendix C. Mathematic derivation of flux decline with respect to foulant accumulation

For simplicity we write $R = R_m + R_f$ in the development of (C2) and (C3). We ignore feed side and draw side external concentration polarization for FO (i.e., equation (C2)) and feed side external concentration polarization for RO (i.e., equation (C3)).

For FO:
$$J = \frac{\pi_{ds}.\exp\left(-\frac{J}{k_{dcp}}\right)-\pi_{fs}}{\mu R} \quad \text{(C1)}$$

Hence for FO the rate of flux decline with respect to fouling is:

$$\frac{dJ}{dR_f} = \frac{-\left(\pi_{ds}.\exp\left(-\frac{J}{k_{dcp}}\right)-\pi_{fs}\right)}{\mu R^2} \Big/ \left[1 + \pi_{ds}.\exp\left(-\frac{J}{k_{dcp}}\right)\Big/ k_{dcp}R\right] \quad \text{(C2)}$$

However for RO the corresponding equation to (C2) is:

$$\frac{dJ}{dR_f} = \frac{-\Delta P}{\mu R^2} \quad \text{(C3)}$$

At the beginning of both experiments $R \approx R_m$ and the only difference between (C2) and (C3), is the denominator in square brackets in (C2). These expressions are related to the gradient of the curves in Fig. 8. The clear implication is that for a given deposition of foulant (equating to a given ΔR) the change in flux will be smaller in FO than in RO. Now foulant accumulation

802 can be expected to continue at a decreasing rate until there is a balance between deposition, by
803 convective flow to and through the membrane, and removal by shear [64]. Now given that flux
804 is declining more slowly with respect to a given amount of foulant accumulation in FO than
805 RO there will naturally be a greater amount of foulant deposition in FO before the limiting flux
806 is reached.
807
808 **Appendix D. Supplementary material**
809 The supplementary data can be found online via the link of http://
810
811
812

Abbreviations

AL–FS	active layer facing feed side
CECP	cake-enhanced concentration polarisation
CEOP	cake-enhanced osmotic pressure
CP	concentration polarisation
CTA	cellulose triacetate
DCP	dilutive concentration polarisation
DI	de-ionised
DS	draw solution
ECP	external concentration polarisation
FO	forward osmosis
FS	feed solution
ICP	internal concentration polarisation
NF	nanofiltration
ODMPs	osmotically driven membrane processes
ORF	osmotic-resistance filtration
RO	reverse osmosis
RSD	reverse solute diffusion

Nomenclature

A	water permeability coefficient (m^3/m^2-Pa)
B	solute permeability coefficient (m^3/m^2)
C	concentration (moles/m^3)
D	diffusion coefficient (m^2/s)
F_{cecp}	concentration polarization factor for CECP (dimensionless)
F_{dcp}	concentration polarization factor for DCP (dimensionless)
F_{ecp}	concentration polarization factor for ECP (dimensionless)
J_s	solute flux (m^3/m^2 s)
J_w	water flux (m^3/m^2 s)
$J_{w,f}$	fouling water flux (m^3/m^2 s)
k	mass transfer coefficient (m/s)
k_{cecp}	mass transfer coefficient near the membrane surface (m/s)
$k_{ecp,f}$	overall mass transfer coefficient across the foulant layer and external concentration polarization boundary layer (m/s)
$k_{ecp,f}^*$	mass transfer coefficient within the foulant layer on the membrane (m/s)
$k_{ecp,o}$	mass transfer coefficient to the ECP boundary layer above the foulant layer (m/s)
M	molar (moles/m^3)
m_f	mass deposition density (g/m^2)
R_f	foulant resistance (m^{-1})
R_f/m_f	specific foulant resistance (m/g)
R_g	universal gas constant (8.3145 m^3 Pa mol^{-1} K^{-1})
R_m	hydraulic resistance of the membrane (m^{-1})
S	structural parameter (m^{-1})

S_f	structural parameter of the foulant layer (m^{-1})
$\overline{S_f}$	overall effective thickness of the CP boundary layer (m)
T	temperature (K)
TMP	transmembrane pressure (Pa)
TOC	total organic carbon (g/m^3)
β	van't Hoff coefficient
δ	boundary layer thickness (m)
μ	fluid viscosity (Pa s)
η_{rej}	solute rejection
π_{ds}	osmotic pressure of the draw solution (Pa)
π_{fs}	osmotic pressure of the feed solution (Pa)
$\pi_{fs,m}$	osmotic pressure of the feed solution at the membrane surface (Pa)
π_i	osmotic pressure of the draw at the interface between the active layer of the membrane and the support
$\Delta\pi$	osmotic pressure difference across the membrane (Pa)
ΔP	effective applied hydraulic pressure (Pa)

References

[1] T.Y. Cath, A.E. Childress, M. Elimelech, Forward osmosis: Principles, applications, and recent developments, J. Membr. Sci., 281 (2006) 70-87.

[2] S. Zhao, L. Zou, C.Y. Tang, D. Mulcahy, Recent developments in forward osmosis: Opportunities and challenges, J. Membr. Sci., 396 (2012) 1-21.

[3] R. Valladares Linares, Z. Li, S. Sarp, S. Bucs, G. Amy, J.S. Vrouwenvelder, Forward osmosis niches in seawater desalination and wastewater reuse, Water Res., 66 (2014) 122-139.

[4] G. Blandin, A. Verliefde, J. Comas, I. Rodriguez-Roda, P. Le-Clech, Efficiently Combining Water Reuse and Desalination through Forward Osmosis—Reverse Osmosis (FO-RO) Hybrids: A Critical Review, Membranes, 6 (2016) 37.

[5] K. Lutchmiah, A.R.D. Verliefde, K. Roest, L.C. Rietveld, E.R. Cornelissen, Forward osmosis for application in wastewater treatment: A review, Water Res., 58 (2014) 179-197.

[6] X. Wang, V.W.C. Chang, C.Y. Tang, Osmotic membrane bioreactor (OMBR) technology for wastewater treatment and reclamation: Advances, challenges, and prospects for the future, J. Membr. Sci., 504 (2016) 113-132.

[7] B.D. Coday, B.G.M. Yaffe, P. Xu, T.Y. Cath, Rejection of Trace Organic Compounds by Forward Osmosis Membranes: A Literature Review, Environmental Science & Technology, 48 (2014) 3612-3624.

[8] X. Wang, J. Zhang, V.W.C. Chang, Q. She, C.Y. Tang, Removal of cytostatic drugs from wastewater by an anaerobic osmotic membrane bioreactor, Chem. Eng. J., 339 (2018) 153-161.

[9] X. Jin, Q. She, X. Ang, C.Y. Tang, Removal of boron and arsenic by forward osmosis membrane: Influence of membrane orientation and organic fouling, J. Membr. Sci., 389 (2012) 182-187.

[10] J. Zhang, Q. She, V.W.C. Chang, C.Y. Tang, R.D. Webster, Mining Nutrients (N, K, P) from Urban Source-Separated Urine by Forward Osmosis Dewatering, Environ. Sci. Technol., 48 (2014) 3386-3394.

[11] A.J. Ansari, F.I. Hai, W.E. Price, J.E. Drewes, L.D. Nghiem, Forward osmosis as a platform for resource recovery from municipal wastewater - A critical assessment of the literature, J. Membr. Sci., 529 (2017) 195-206.

[12] S. Phuntsho, H.K. Shon, S. Hong, S. Lee, S. Vigneswaran, A novel low energy fertilizer driven forward osmosis desalination for direct fertigation: Evaluating the performance of fertilizer draw solutions, J. Membr. Sci., 375 (2011) 172-181.

[13] D.L. Shaffer, J.R. Werber, H. Jaramillo, S. Lin, M. Elimelech, Forward osmosis: Where are we now?, Desalination, 356 (2015) 271-284.

[14] L. Chekli, S. Phuntsho, J.E. Kim, J. Kim, J.Y. Choi, J.-S. Choi, S. Kim, J.H. Kim, S. Hong, J. Sohn, H.K. Shon, A comprehensive review of hybrid forward osmosis systems: Performance, applications and future prospects, J. Membr. Sci., 497 (2016) 430-449.

[15] R.K. McGovern, J.H. Lienhard V, On the potential of forward osmosis to energetically outperform reverse osmosis desalination, J. Membr. Sci., 469 (2014) 245-250.

[16] N.M. Mazlan, D. Peshev, A.G. Livingston, Energy consumption for desalination — A comparison of forward osmosis with reverse osmosis, and the potential for perfect membranes, Desalination, 377 (2016) 138-151.

[17] T.-S. Chung, L. Luo, C.F. Wan, Y. Cui, G. Amy, What is next for forward osmosis (FO) and pressure retarded osmosis (PRO), Sep. Purif. Technol., 156 (2015) 856-860.

[18] A. Achilli, T.Y. Cath, E.A. Marchand, A.E. Childress, The forward osmosis membrane bioreactor: A low fouling alternative to MBR processes, Desalination, 238 (2009) 10-21.

[19] B. Mi, M. Elimelech, Organic fouling of forward osmosis membranes: Fouling reversibility and cleaning without chemical reagents, J. Membr. Sci., 348 (2010) 337-345.

[20] S. Lee, C. Boo, M. Elimelech, S. Hong, Comparison of fouling behavior in forward osmosis (FO) and reverse osmosis (RO), J. Membr. Sci., 365 (2010) 34-39.
[21] B. Mi, M. Elimelech, Silica scaling and scaling reversibility in forward osmosis, Desalination, 312 (2013) 75-81.
[22] Y. Kim, M. Elimelech, H.K. Shon, S. Hong, Combined organic and colloidal fouling in forward osmosis: Fouling reversibility and the role of applied pressure, J. Membr. Sci., 460 (2014) 206-212.
[23] S.E. Kwan, E. Bar-Zeev, M. Elimelech, Biofouling in forward osmosis and reverse osmosis: Measurements and mechanisms, J. Membr. Sci., 493 (2015) 703-708.
[24] M. Xie, J. Lee, L.D. Nghiem, M. Elimelech, Role of pressure in organic fouling in forward osmosis and reverse osmosis, J. Membr. Sci., 493 (2015) 748-754.
[25] F. Lotfi, L. Chekli, S. Phuntsho, S. Hong, J.Y. Choi, H.K. Shon, Understanding the possible underlying mechanisms for low fouling tendency of the forward osmosis and pressure assisted osmosis processes, Desalination, (2017).
[26] Y. Yu, S. Lee, S.K. Maeng, Forward osmosis membrane fouling and cleaning for wastewater reuse, Journal of Water Reuse and Desalination, 7 (2017) 111-120.
[27] J. Lee, S. Kook, C. Lee, I.S. Kim, Effect of intermittent pressure-assisted forward osmosis (I-PAFO) on organic fouling, Desalination, 419 (2017) 60-69.
[28] G. Blandin, A.R.D. Verliefde, P. Le-Clech, Pressure enhanced fouling and adapted anti-fouling strategy in pressure assisted osmosis (PAO), J. Membr. Sci., 493 (2015) 557-567.
[29] W.C.L. Lay, T.H. Chong, C.Y. Tang, A.G. Fane, J. Zhang, Y. Liu, Fouling propensity of forward osmosis: Investigation of the slower flux decline phenomenon, Water Sci. Technol., 61 (2010) 927-936.
[30] Y. Jang, H. Cho, Y. Shin, Y. Choi, S. Lee, J. Koo, Comparison of fouling propensity and physical cleaning effect in forward osmosis, reverse osmosis, and membrane distillation, Desalination and Water Treatment, 57 (2016) 24532-24541.
[31] E.W. Tow, J.H. Lienhard V, Quantifying osmotic membrane fouling to enable comparisons across diverse processes, J. Membr. Sci., 511 (2016) 92-107.
[32] A.G. Fane, T.H. Chong, J. Zhang, W.C.L. Lay, The Effect of Flux and Pressure on Fouling in Reverse Osmosis Desalination, Proceedings IDA World Congress, (2009) Paper DB09-128.
[33] R.W. Field, G.K. Pearce, Critical, sustainable and threshold fluxes for membrane filtration with water industry applications, Adv. Colloid Interface Sci., 164 (2011) 38-44.
[34] Z. Xie, N. Nagaraja, L. Skillman, D. Li, G. Ho, Comparison of polysaccharide fouling in forward osmosis and reverse osmosis separations, Desalination, 402 (2017) 174-184.
[35] J.R. McCutcheon, M. Elimelech, Influence of concentrative and dilutive internal concentration polarization on flux behavior in forward osmosis, J. Membr. Sci., 284 (2006) 237-247.
[36] C.Y. Tang, Q. She, W.C.L. Lay, R. Wang, A.G. Fane, Coupled effects of internal concentration polarization and fouling on flux behavior of forward osmosis membranes during humic acid filtration, J. Membr. Sci., 354 (2010) 123-133.
[37] Q. She, R. Wang, A.G. Fane, C.Y. Tang, Membrane fouling in osmotically driven membrane processes: A review, J. Membr. Sci., 499 (2016) 201-233.
[38] E.M.V. Hoek, M. Elimelech, Cake-Enhanced Concentration Polarization: A New Fouling Mechanism for Salt-Rejecting Membranes, Environ. Sci. Technol., 37 (2003) 5581-5588.
[39] T.H. Chong, F.S. Wong, A.G. Fane, Implications of critical flux and cake enhanced osmotic pressure (CEOP) on colloidal fouling in reverse osmosis: Experimental observations, J. Membr. Sci., 314 (2008) 101-111.
[40] C.Y. Tang, Y.N. Kwon, J.O. Leckie, Characterization of humic acid fouled reverse osmosis and nanofiltration membranes by transmission electron microscopy and streaming potential measurements, Environ. Sci. Technol., 41 (2007) 942-949.

[41] A. Tiraferri, N.Y. Yip, A.P. Straub, S. Romero-Vargas Castrillon, M. Elimelech, A method for the simultaneous determination of transport and structural parameters of forward osmosis membranes, J. Membr. Sci., 444 (2013) 523-538.
[42] A.J. Karabelas, D.C. Sioutopoulos, Toward improvement of methods for predicting fouling of desalination membranes — The effect of permeate flux on specific fouling resistance, Desalination, 343 (2014) 97-105.
[43] Q. She, Y.K.W. Wong, S. Zhao, C.Y. Tang, Organic fouling in pressure retarded osmosis: Experiments, mechanisms and implications, J. Membr. Sci., 428 (2013) 181-189.
[44] Q. She, X. Jin, Q. Li, C.Y. Tang, Relating reverse and forward solute diffusion to membrane fouling in osmotically driven membrane processes, Water Res., 46 (2012) 2478-2486.
[45] Q. She, D. Hou, J. Liu, K.H. Tan, C.Y. Tang, Effect of feed spacer induced membrane deformation on the performance of pressure retarded osmosis (PRO): Implications for PRO process operation, J. Membr. Sci., 445 (2013) 170-182.
[46] E.M.V. Hoek, A.S. Kim, M. Elimelech, Influence of crossflow membrane filter geometry and shear rate on colloidal fouling in reverse osmosis and nanofiltration separations, Environmental Engineering Science, 19 (2002) 357-372.
[47] C.Y. Tang, T.H. Chong, A.G. Fane, Colloidal interactions and fouling of NF and RO membranes: A review, Adv. Colloid Interface Sci., 164 (2011) 126-143.
[48] R.W. Field, J.J. Wu, Mass transfer limitations in forward osmosis: Are some potential applications overhyped?, Desalination, 318 (2013) 118-124.
[49] T.Y. Cath, M. Elimelech, J.R. McCutcheon, R.L. McGinnis, A. Achilli, D. Anastasio, A.R. Brady, A.E. Childress, I.V. Farr, N.T. Hancock, J. Lampi, L.D. Nghiem, M. Xie, N.Y. Yip, Standard Methodology for Evaluating Membrane Performance in Osmotically Driven Membrane Processes, Desalination, (2012).
[50] B. Kim, G. Gwak, S. Hong, Review on methodology for determining forward osmosis (FO) membrane characteristics: Water permeability (A), solute permeability (B), and structural parameter (S), Desalination, 422 (2017) 5-16.
[51] B. Mi, M. Elimelech, Gypsum scaling and cleaning in forward osmosis: Measurements and mechanisms, Environ. Sci. Technol., 44 (2010) 2022-2028.
[52] L. Song, M. Elimelech, Particle Deposition onto a Permeable Surface in Laminar Flow, J. Colloid Interface Sci., 173 (1995) 165-180.
[53] L.N. Sim, Y. Ye, V. Chen, A.G. Fane, Investigations of the coupled effect of cake-enhanced osmotic pressure and colloidal fouling in RO using crossflow sampler-modified fouling index ultrafiltration, Desalination, 273 (2011) 184-196.
[54] C.Y. Tang, J.O. Leckie, Membrane independent limiting flux for RO and NF membranes fouled by humic acid, Environ. Sci. Technol., 41 (2007) 4767-4773.
[55] E.W. Tow, J.H. Lienhard V, Unpacking compaction: Effect of hydraulic pressure on alginate fouling, J. Membr. Sci., 544 (2017) 221-233.
[56] A. Rushton, A.S. Ward, R.G. Holdich, Solid-Liquid Filtration and Separation Technology, Wiley-VCH, 1996.
[57] R. Guha, X. Shang, A.L. Zydney, D. Velegol, M. Kumar, Diffusiophoresis contributes significantly to colloidal fouling in low salinity reverse osmosis systems, J. Membr. Sci., 479 (2015) 67-76.
[58] M. Zhang, D. Hou, Q. She, C.Y. Tang, Gypsum scaling in pressure retarded osmosis: Experiments, mechanisms and implications, Water Res., 48 (2014) 387-395.
[59] M. Zhang, Q. She, X. Yan, C.Y. Tang, Effect of reverse solute diffusion on scaling in forward osmosis: A new control strategy by tailoring draw solution chemistry, Desalination, 401 (2017) 230-237.

[60] P. van den Brink, A. Zwijnenburg, G. Smith, H. Temmink, M. van Loosdrecht, Effect of free calcium concentration and ionic strength on alginate fouling in cross-flow membrane filtration, J. Membr. Sci., 345 (2009) 207-216.
[61] S. Meng, Y. Liu, Transparent exopolymer particles (TEP)-associated membrane fouling at different Na+ concentrations, Water Res., 111 (2017) 52-58.
[62] J. BAUMY, J., G. BRULE, Effect of pH and ionic strength on the binding of bivalent cations to β-casein, Lait, 68 (1988) 409-417.
[63] K.J. Thomas, C.V. Rice, Revised model of calcium and magnesium binding to the bacterial cell wall, BioMetals, 27 (2014) 1361-1370.
[64] R.W. Field, J.J. Wu, Modelling of permeability loss in membrane filtration: Re-examination of fundamental fouling equations and their link to critical flux, Desalination, 283 (2011) 68-74.